Design strategy and simulation of medium-frequency transformers for a three-phase dual active bridge

Tobias Kauder and Kay Hameyer
Institute of Electrical Machines (IEM)
RWTH Aachen University
Aachen, Germany
tobias.kauder@iem.rwth-aachen.de

Thierry Belgrand
thyssenkrupp Electrical Steel UGO
Rue Roger Salengro
Isbergues, France
thierry.belgrand@thyssenkrupp.com

***Abstract*— Transformers are key elements in high power dc/dc converters such as the dual active bridge. Special attention is required because the dc-to-dc technique operates with non-sinusoidal voltages and currents. Therefore, iron and copper losses differ when compared to standard ac (sinusoidal) operation and sinus based design rules are no more suitable. The working principle of a dual active bridge (DAB3) relies on a particular value of leakage inductance to control the power flow. This inductance can be realized by the sole leakage inductance of the transformer or by connecting an additional choke inductance. The present paper shows the results obtained using an evolutionary strategy applied to design a transformer. The algorithm is adjusted to the particular conditions of the converter such as the flux density waveform (DAB3). The integration of the inductance can be performed by the design strategy and the design is compared to the external choke inductance solution. At this stage of work, the overall test bench setup is verified using simulations.**

Keywords*— *transformers, medium-frequency, evolutionary strategy, magnetic measurements, electric circuit simulation, dual active bridge, high power dc/dc converter

I. Introduction

Medium-frequency transformers are used in high-power dc/dc converters when galvanic insulation between transformer input and output is required. The design of such transformers is different from the common high-power grid transformers as well as to the ones in small power dc/dc converters. Classical design rules from literature are not applicable, because the conditions inside the converter are away from sinusoidal operation. In a dual active bridge, non-sinusoidal excitation effects on the core and the winding are to be considered. The resulting influences need to be known during the designing process. The main effects depend on the applied materials and the occurring changes in any of them should feedback to a modified converter operating point and an adapted component design. On the one hand, a transformer design is possible by scaling rules [1, 2] or by modification of common designs rules [3]. In this case, the design process strongly depends on the experience of the engineer and optimization concerning a particular application is difficult [4]. On the other hand, numerical search algorithms such as design of experiments, particle swarm or evolutionary strategies can evaluate large regions of design parameter combinations. The high number of design variables such as geometric dimensions, number of turns as well as the used materials can be formulated as an optimization problem to evaluate various regions of possible designs [5–9]. In this paper, an evolutionary design strategy is discussed to include the non-sinusoidal conditions during the transformer design process. Pareto-optimal designs are chosen with integrated and external inductance. The advantages and disadvantages of increased leakage are evaluated. The contributions of this paper are:

- Draft of the test bench including the requirements on the transformer. (Section 2)
- Transformer model. (Section 3)
- Evolutionary strategy. (Section 4)
- Pareto Front and evidence of the proposed design by simulation of load case. (Section 5)

II. Converter Test Bench Design

The three-phase dual active bridge [10] is capable of large power transfer and it benefits from reduced switching operations and soft-switching capabilities. One experimental transformer design with 200 kVA is in focus to establish a bidirectional power flow between two 600 V dc-links. The specifications are listed in TABLE I. Fig. 1 shows the topology, the transformer and the inductance in a schematic view. In this converter, a six-step voltage waveform is applied to the transformer. The power flow is controlled by a phase shift between primary and secondary side. The switching frequency of the semiconductors equals the fundamental frequency of the transformer. This reduces the switching operations and losses compared to PWM techniques and the converter can work at increased frequencies, allowing much smaller, lighter and cheaper electromagnetic components.

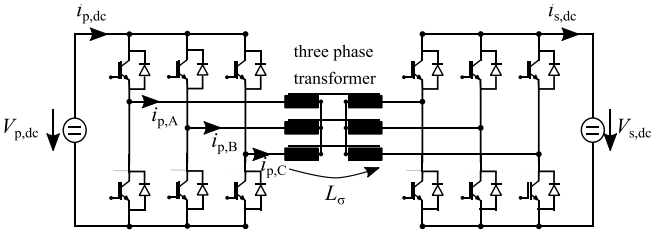

Fig. 1. Dual active bridge topology with transformer.

TABLE I. SPECIFICATIONS.

Variable	Value	Description
S_n	200 kVA	Apparent power
P_n	150 kW	Active power
$V_{p,dc}$	600 V	Dc link voltage
$V_{s,dc}$	600 V	Dc link voltage
C	1 mF	Dc link capacitances

The switching frequency of the converter is chosen as a degree of freedom in the design and should be determined after studying the efficiency and the resulting transformer designs. The main idea of this paper is to design one transformer for the described test bench setup with respect to optimal working point for the studied core material.

III. THREE-PHASE TRANSFORMER MODEL

A three-limb stacked core layout made of 0.18 mm thick High Permeability Grain Oriented Electrical Steel (GOES) with aluminum foil windings is studied. The increased frequency is meant to achieve volume reduction but the impact on consequent increased specific losses of the core material has to be considered. The choice of dimensions and parameters is a multi-component problem and depends on overall efficiency, frequency and required total active mass.

A. Soft magnetic material

Metrological characterization of GOES was performed with dedicated measurement instruments. A single-sheet-tester (SST) from Brockhaus Measurement Systems is equipped with a 120 x 120 mm specimen. The magnetic field is applied along the easy magnetization axis (Rolling Direction) of the sample and the magnetic polarization along that same axis is assessed. Measurements with controlled DAB3 conditions were performed based on the principle described by the international standard IEC 60404-3 [11]. The measured permeability values and the iron losses are used in the design process.

B. Geometry of core and windings

The magnetic core complexity (geometry and nonlinear magnetic properties) is translated by segmenting the various elements into a reluctance network. Look-up tables provide the magnetic permeability μ as a function of frequency f and magnetic flux density B. A rectangular core shape is considered and the cross sectional area is chosen as constant for the total core. An air gap is included in the magnetic resistance of each transformer limb. The structures of the core joints were not modeled in detail. The algorithm adjusts the continuous parameter of length l, width w and depth d of each reluctance $\mathcal{R}$:

$$\mathcal{R} = \frac{l}{\mu(f,B)\ A} = \frac{l}{\mu(f,B)\ w\ d} \quad . \tag{1}$$

The total reluctance per phase A, B or C results from series and parallel connection of the reluctance network in Fig. 2.

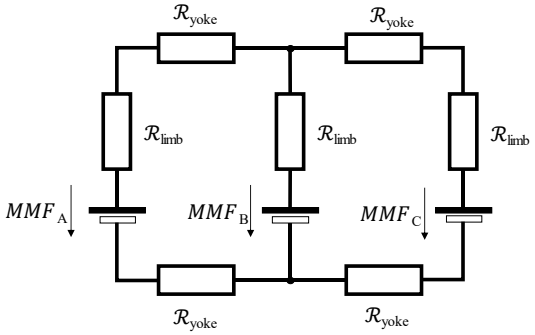

Fig. 2. Three leg transformer equivalent reluctance circuit.

The conductors are aluminum foil windings with elliptic cylinder shapes. Aluminum is chosen to reduce weight and to decrease eddy current winding losses. The width of each coil is calculated by the number of turns N and the insulation layers. The 2D partial view in Fig. 3 shows the geometric variables, which are adjusted by the algorithm. The parameters are listed in TABLE II. The material properties are listed in TABLE III.

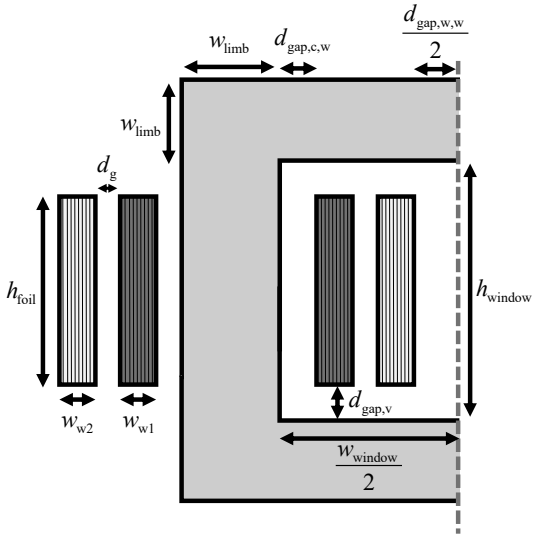

Fig. 3. Core-type transformer. Dimensions and clearances between the components. 2D partial view.

C. Leakage inductance

Analytical calculation of the leakage inductance (2) includes the Rogowski factor [12] ($K_R < 1$). The geometry of the windings and the gap is considered in the mean diameters D_{w1}, D_{w2} and D_g. The parameters w_{w1}, w_{w2} and d_g are the thicknesses of each component.

$$L_\sigma = \frac{\mu_0 N^2 \pi}{h_{foil} / K_R} \left(\frac{w_{w1} D_{w1}}{3} + d_g D_g + \frac{w_{w2} D_{w2}}{3} \right) \tag{2}$$

This formula corrects the presence of a vertical gap between core and windings $d_{\mathrm{gap,v}}$ by adjusting the length of the leakage flux lines [13]. Theoretically, high number of turns N or increased radial winding dimensions yields to higher leakage. This approach will be used to increase the internal leakage inductance in case of high internal leakage designs.

TABLE II. INPUT PARAMETERS AND RANGE OF VALUES.

set of design parameters		range of values
w_{limb}	limb and yoke width	10 mm < w_{limb} < 200 mm
l_{limb}	limb length	50 mm < l_{limb} < 1.75 m
d_{limb}	limb and yoke depth	15 mm < d_{limb} < 250 mm
h_{foil}	foil height	h_{foil} < 1.5 m
N_1=N_2	number of turns	1 < N < 200
d_g	winding gap	5 mm < d_{g}
$d_{\mathrm{gap,v}}$	vertical clearance	5 mm < $d_{\mathrm{gap,v}}$
$d_{\mathrm{gap,c,w}}$	core clearance	5 mm < $d_{\mathrm{gap,c,w}}$
$d_{\mathrm{gap,w,w}}$	clearance between phases	5 mm < $d_{\mathrm{gap,w,w}}$

D. Core losses

The iron loss formula [14] developed for Non Grain Oriented Electrical Steel is based on semi-physical parameters and was adjusted to fit GOES properties. It is used to evaluate the material characteristics and to describe the measured iron losses. A fitting process, based on quasi static and high frequency measurements, determines the parameters. The parameters correspond to the hysteresis, eddy current, excess and nonlinear loss components of the studied GOES.

E. Winding losses

Foil conductor resistances are approximated according to Dowels equations [15]. The classical R_{DC} resistance is calculated and adjusted with the ac-to-dc resistance increase factor F_{R}. Since the geometry of the core is calculated at first, the linear solved magnetizing current is added to the winding losses. The harmonic contents of the load current were simulated in advance [16] and the losses P_{w} are calculated for primary and secondary side using fast Fourier transform (FFT):

$$P_{\mathrm{w}} = F_r \, R_{DC} \sum_i I_i^2 \quad . \tag{3}$$

F. Temperature

The temperatures occur because of resulting losses and the heat dissipation is considered on core and winding surfaces. A heat flux $\dot{Q}$ is resulting from the generated losses and the rise of temperature ΔT must not exceed the insulation limits (4) of each component. Temperature Class 250 as defined in [17] is considered by air-forced convective heat transfer coefficients h. The optimized designs required a sufficient amount of surface for core and windings to dissipate the internal heat. The geometries and corresponding surfaces A are represented using thermal resistances networks [18] for the studied materials and cooling method:

$$\dot{Q} = h A \, \Delta T \quad . \tag{4}$$

TABLE III. GENERAL MATERIAL PROPERTIES.

t_{GOES}	0.18 mm	GOES nominal thickness
ρ_{fe}	7650 kg/m^3	GOES conventional density
ρ_{Al}	2800 kg/m^3	Winding material density
α_{Al}	0.004308 1/K	Temperature coefficient of winding material

IV. EVOLUTIONARY STRATEGY

The design and optimization, subject to weight and losses, is performed for a three-phase transformer by applying a meta-heuristic evolutionary strategy [19] matching the specifications. The resulting designs vary in active mass m or in generated losses P. The resulting mass and losses are used for the multi-objective optimization strategy (8). With this approach a Pareto-Front is generated which consists of different designs. A mixed-integer approach is used to include the continuous parameter solution space such as the length and width of core dimensions as well as integer problems such as the number of primary and secondary turns. Each design represents a vector of input parameters:

$$\mathbf{x}^{\mathrm{i}} = \left[w^{\mathrm{i}}_{\mathrm{limb}} \; l^{\mathrm{i}}_{\mathrm{limb}} \; d^{\mathrm{i}}_{\mathrm{limb}} \; w^{\mathrm{i}}_{\mathrm{window}} \; d^{\mathrm{i}}_{\mathrm{gap,c,w}} \; h^{\mathrm{i}}_{foil} \; N^i \ldots f_{el} \right]^T \quad . \tag{5}$$

Based on this parameter set of the ith member of the population, the objective function is evaluated:

$$\begin{bmatrix} f_1 \\ f_2 \end{bmatrix}^{\mathrm{i}} = \mathrm{f}\left(\mathbf{x}^{\mathrm{i}}\right) \quad . \tag{6}$$

A. Constraints

During the strategy, designs are generated and their geometry and losses is calculated. The implemented constraints C serve as a feedback to the algorithm.

$$\bar{c} = \frac{1}{C} \sum_{i=1}^{C} c_{\mathrm{i}} \tag{7}$$

For example, the winding area cannot exceed half the available window area and the device temperature should not exceed the temperature limit. If an individual does not pass a particular constrain, c_{i} (7) will be less than one and the optimization function will return a negative value linear to the number the particular constraint.

TABLE IV. CONSTRAINTS.

design results	limits
Temperature limit	$\Delta T < 250$ °C
Window width	$d_{\mathrm{gap,c,w}} + w_{\mathrm{w1}} + d_{\mathrm{g}} + w_{\mathrm{w2}} + \frac{d_{\mathrm{gap,w,w}}}{2} \leq \frac{w_{\mathrm{window}}}{2}$
Foil height	$h_{\mathrm{foil}} + 2\, d_{\mathrm{gap,v}} \leq l_{\mathrm{limb}}$
Flux density	$0.1\ \mathrm{T} < B < 2.0\ \mathrm{T}$
Leakage inductance	$L_{\mathrm{min}} < L_{\sigma} < L_{\mathrm{max}}$

B. *Optimization function*

For the multi-objective problem, the optimization function is:

$$f = \begin{cases} \varepsilon\left(\bar{c} - 1\right)\begin{bmatrix} 1 & 1 \end{bmatrix}^T, & \bar{c} < 1 \\ \begin{bmatrix} \frac{1}{m} & \frac{1}{P} \end{bmatrix}^T, & \bar{c} = 1 \end{cases} . \tag{8}$$

This approach allows multiple constraints in the design algorithm and the total mass and total losses of a valid design are minimized in the global process of maximizing the optimization function.

V. RESULTS

A. *Pareto-Front with minimized leakage*

The Pareto fronts are shown in Fig. 4 (a) for designs with an excitation frequency of $f = 500$ Hz, 1000 Hz and 2000 Hz. For each frequency, multiple designs can be considered. The multi-objective Pareto Front lists devices with minimized loss and mass. A comparison of the studied excitation frequencies shows that a frequency of $f = 1000$ Hz results in the most compacts designs with the lowest losses. Due to the specifications, an excitation of $f = 500$ Hz as well as $f = 2000$ Hz results in having designs with larger active mass in case of the same assumed losses or in higher losses in case of the same active mass.

As a result, high excitation frequencies can be used to reduce the active mass and to increase the efficiency. However, the cooling system must be designed and adapted to dissipate the generated losses.

In Fig. 4 (b), the peak flux density of each design is shown. The GOES material has a high permeability (some ten thousands) up to approximately $B = 1.9$ T. In order to build a compact design and to involve the core material at its best, a high flux density is preferred. This reduces the required cross sectional core area and the active mass. At $f = 500$ Hz, the range of flux density is up to $B = 2.0$ T, at $f = 1000$ Hz up to $B = 1.5$ T and at $f = 2000$ Hz up to $B = 0.75$ T with a state of the art cooling system dissipating the generated losses. These values of flux density can be increased in case of better cooling concepts and by choosing a different power and voltage level. In order to build a compact transformer and to utilize the high permeability soft magnetic material, a frequency of $f = 1000$ Hz is chosen as a compromise. The combination of frequency and a high flux density of $B = 1.5$ T will reduce the core weight. A prototype is planned based on this design. The high permeability and low thickness of the used GOES grade will result in low magnetizing currents.

B. *Pareto-Front with increased leakage inductance*

The required inductance (9) depends on the specifications such as voltage level $V_{\mathrm{p,DC}}$, nominal active power P_{n} and the electrical frequency f of the dual active bridge. According to [20], the size of the leakage inductance depends on the nominal phase shift φ . The phase shift is set to $\varphi = 30°$:

$$L_{\sigma} = 0.27 \cdot \frac{V_{\mathrm{p,DC}}^2}{2\pi f P_{\mathrm{n}}} \frac{7\pi}{36} . \tag{9}$$

The losses of all designs in Fig. 5 (a) are increased compared to Fig. 4 (a). Due to the additional design condition, the evolutionary strategy generates modified designs. The number of turns and the distance between the windings is increased to reach the required leakage, which results in higher conductor losses and increased active mass. The designs have a larger winding-window and increased core

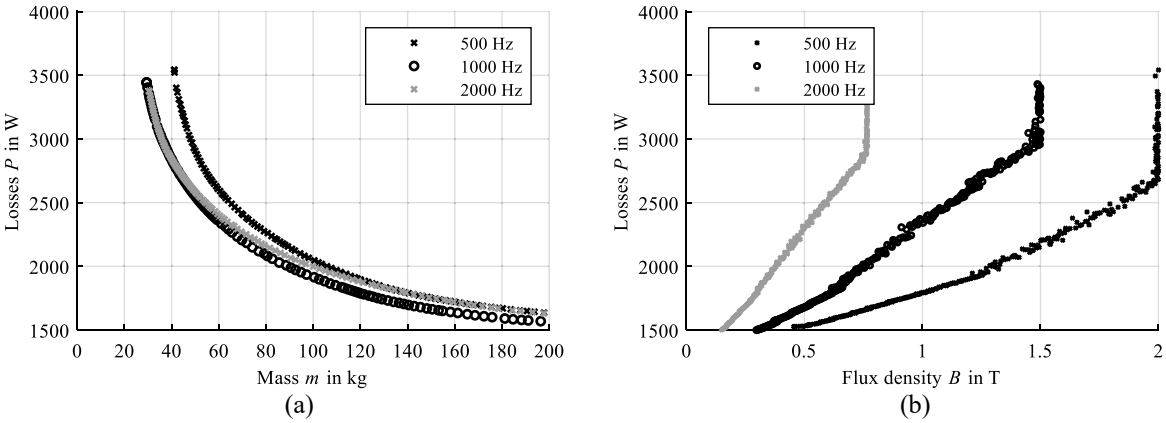

Fig. 4. Transformer design with minimal leakage for different frequencies *f*. Calculations over 1500 generations with a population of 300. Conductor and iron losses versus active mass (Pareto front) (a) and flux density distribution of the proposed designs (b).

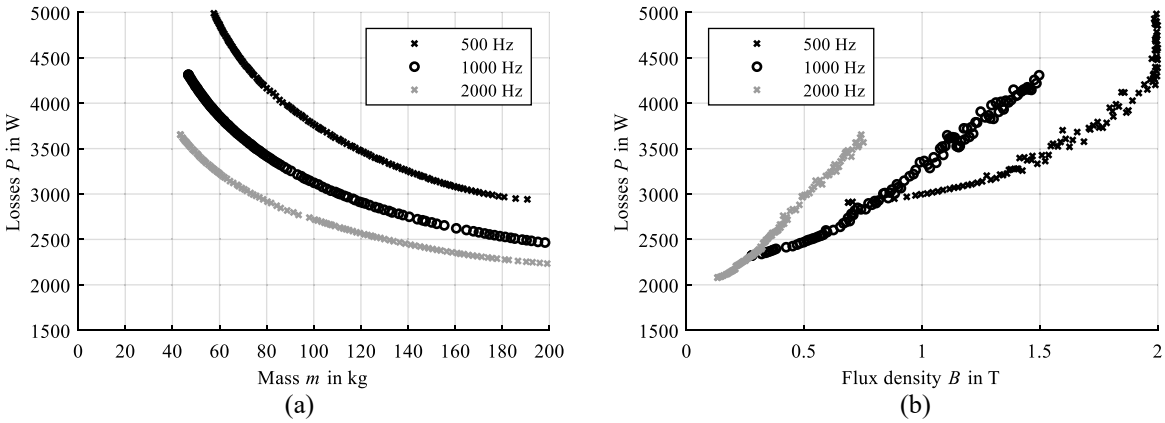

Fig. 5. Transformer design with high leakge L_σ for different frequencies *f*. Calculations over 1500 generations with a population of 300. Conductor and iron losses versus active mass (Pareto front) (a) and flux density distribution of the proposed designs (b).

dimensions. The required leakage inductance decreases with increasing frequency (10). Therefore, the $f = 500$ Hz designs require more leakage flux to operate in a dual active bridge and the target value for the designs is $L_{\sigma,500\ Hz} = 249$ µH. The designs at $f = 1000$ Hz require a leakage inductance of $L_{\sigma,1000\ Hz} = 124$ µH and the $f = 2000$ Hz designs require $L_{\sigma,2000\ Hz} = 62$ µH. Compared to the reference designs in Fig. 4 (a), the ones with internal leakage show increased losses as well as increased active mass. This is due to the additional number of turns and the increased coil volumes.

In the case of higher frequencies, the required leakage inductance (9) is smaller. Theoretically, the requested leakage could be realized at high frequency designs as internal leakage inductance. As a result, the designs require minimum 20 % more active mass and the losses are increased by approx. 15 %. In Fig. 5 (b), the magnetic flux density of each design is shown for the considered specifications and cooling system. Two designs are compared in TABLE V: One $f = 1000$ Hz design with minimized leakage Fig. 6 (a) — in this case the necessary leakage inductance is provided by an external air choke inductance — and one design with the required internal leakage Fig. 6 (b). As a result, the design with increased leakage has an increased number of turns to fit the targeted leakage value. This results in higher winding resistance (copper losses) and increased total mass. The core area has been adjusted to keep the same voltage level at the same peak flux density of $B = 1.5$ T. To conclude, the system with external choke inductance shows the better efficiency for transformers designed with the chosen GOES material.

TABLE V. DESIGN SUMMARY.

Design proposals. Minimal and high leakage.			
L_σ	Leakage inductance	30.2 µH	123.4 µH
f	Electrical frequency	1000 Hz	1000 Hz
A	Cross sectional core area	18.4 cm^2	14.3 cm^2
B	Flux density	1.5 T	1.5 T
N	Number of turns	24	32
P_w	Winding losses	1873 W	3154 W
P_{fe}	Core losses	1288 W	1143 W
P_{igbt}	IGBT losses	1870 W	1870 W
m	Transformer mass	36.4 kg	46.8 kg

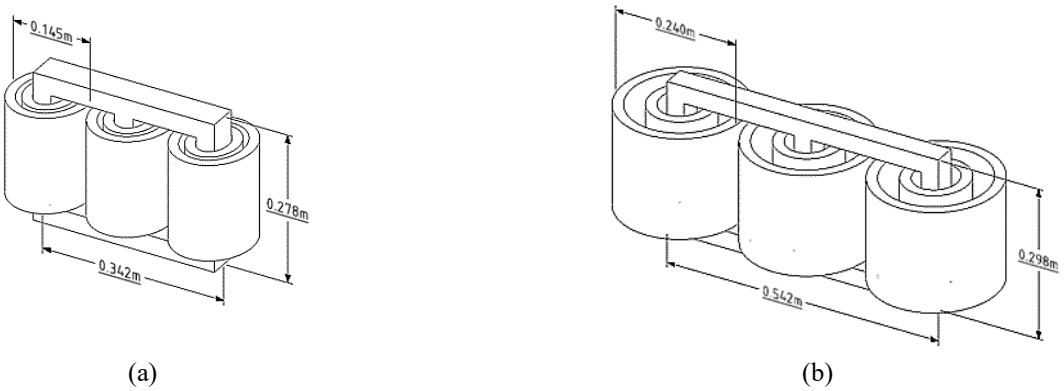

Fig. 6. 3D geometries. Compact 1000 Hz designs. Minimized leakage (a) and increased leakage (b). The design with increased leakage results in more losses and active mass.

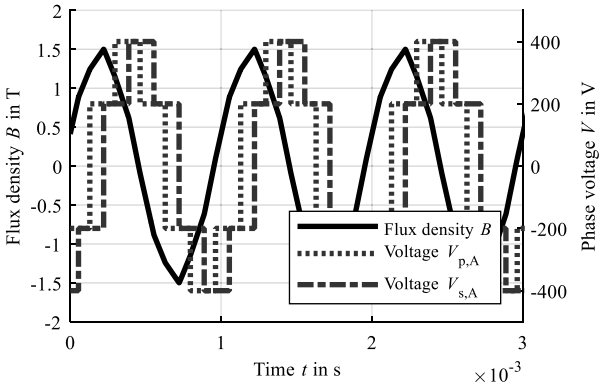

Fig. 7. The core flux density simulation in phase A. To transmit nominal power, the secondary winding voltage $V_{s,A}$ is applied with a phase shift of $\varphi = 30°$ with respect to the primary winding voltage $V_{p,A}$.

In Fig.7 the simulated flux density is shown for the design with external choke inductance on the primary side to fulfil the working principle of the dual active bridge. The choke inductance results in an different phase shift between flux density B and primary voltage $V_{p,A}$ compared to the phase shift between flux density B and secondary voltage $V_{s,A}$.

VI. Conclusions

A multi-objective evolutionary strategy was used to evaluate medium-frequency transformer designs. The increase of frequency has an impact on the occurring specific losses. Therefore, a thermal model was implemented to study the resulting winding and core temperatures. In this study, the high magnetic saturation and high permeability of the material resulted in compact medium frequency transformers with low magnetizing currents. The ability of the used GOES grade to be magnetized at high induction level combined to reduced thickness (0.18 mm) of the studied GOES material resulted in reduced eddy current core losses for the chosen working induction level. The measured properties of the material were employed in an evolutionary strategy to design a transformer to the given specifications. A f = 1000 Hz design with B = 1.5 T was compared between solutions with external or integrated leakage inductance. The higher the frequency the lower is the required leakage. In case of integrated leakage inductance, the number of turns and the distance between the windings are increased to reach the targeted leakage value. This resulted in minimum 15% more losses and minimum 20% more active mass of the device compared to an external leakage inductance. Due to this, we focus on an additional choke inductance solution to benefit from the material performance at high induction levels. In a next step of this study, we will focus on building the transformer based on the discussed f = 1000 Hz and B = 1.5 T design.

Acknowledgement

This work is sponsored by thyssenkrupp Electrical Steel GmbH.

References

[1] R. Chattopadhyay, M. A. Juds, P. R. Ohodnicki and S. Bhattacharya, "Modelling, design and analysis of three limb high frequency transformer including transformer parasitics, for SiC Mosfet based three port DAB, IECON 2016 - 42nd Annual Conference of the IEEE Industrial Electronics Society: IEEE, 2016, pp. 4181–4186.

[2] C. W. T. McLyman, Transformer and Inductor Design Handbook, Fourth Edition, 4th ed. Hoboken, Taylor and Francis, 2011.

[3] R. Petkov, "Optimum design of a high-power, high-frequency transformer", IEEE Transactions on Power Electronics, vol. 11, No. 1, pp. 33–42, 1996.

[4] U. Pahner, K. Hameyer and R. Belmans, "A parallel implementation of a parametric optimization environment-numerical optimization of an inductor for traction drive systems", IEEE Trans. On energy Conversion, vol. 14, No. 4, pp. 1329–1334, 1999.

[5] Y. Xu, L. X. Chen, W. Z. Guo, K. W. He and J. X. Zuo, "Optimal design of high-frequency Fe-based amorphous transformer based on genetic algorithm", International Conference on Pulsed Power, pp. 1–4.

[6] L. Zhang, D. Zhang, H. Shui, Y. Yuan, Q. Pei and J. Zhu, "Optimisation design of medium frequency transformer for the offshore dc grid based on multi-objective genetic algorithm", Institution of Engineering and Technology Power Electronics, vol. 10, No. 15, pp. 2157–2162, 2017.

[7] E. I. Amoiralis, M. A. Tsili and A. G. Kladas, "Global transformer design optimization using deterministic and non-deterministic algorithms", International Conference on Electrical Machines (ICEM), pp. 2323–2331, 2012.

[8] E. I. Amoiralis, P. S. Georgilakis, M. A. Tsili and A. G. Kladas, "Global Transformer Optimization Method Using Evolutionary Design and Numerical Field Computation", IEEE Trans. Magn, vol. 45, No. 3, pp. 1720–1723, 2009.

[9] L. D. S. Coelho, V. C. Mariani, F. A. Guerra, M. V. F. da Luz and J. V. Leite, "Multiobjective Optimization of Transformer Design Using a Chaotic Evolutionary Approach", IEEE Trans. Magn, vol. 50, No. 2, pp. 669–672, 2014.

[10] R. W. De Doncker, D. M. Divan and M. H. Kheraluwala, "A three-phase soft-switched high-power-density DC/DC converter for high-power applications", IEEE Transactions on Industry Applications, vol. 27, No. 1, pp. 63–73, 1991.

[11] Magnetic materials – Part 3: Methods of measurement of the magnetic properties of electrical steel strip and sheet by means of a single sheet tester, IEC 60404-3, 2010.

[12] S. V. Kulkarni and S. A. Khaparde, Transformer engineering, Design and practice. New York, Marcel Dekker, 2004.

[13] R. Doebbelin, C. Teichert, M. Benecke and A. Lindemann, "Computerized Calculation of Leakage Inductance Values of Transformers", Progress In Electromagnetics Research Symposium Proceedings, Cambridge, pp. 439–443, 2010.

[14] D. Eggers, S. Steentjes and K. Hameyer, "Advanced Iron-Loss Estimation for Nonlinear Material Behavior", IEEE Transactions on Magnetics, vol. 48, No. 11, pp. 3021–3024, 2012.

[15] P. L. Dowell, "Effects of eddy currents in transformer windings", Proceedings of the Institution of Electrical Engineers, vol. 113, No. 8, pp. 1387–1394, 1966.

[16] I. Villar, L. Mir, I. Etxeberria-Otadui, J. Colmenero, X. Agirre and T. Nieva, "Optimal design and experimental validation of a Medium-Frequency 400kVA power transformer for railway traction applications", IEEE Energy Conversion Congress and Exposition (ECCE), 2012.

[17] Electrical insulation - Thermal evaluation and designation, IEC 60085, 2007.

[18] U. Drofenik, "A 150kW Medium Frequency Transformer Optimized for Maximum Power Density", Integrated Power Electronics Systems, 2012.

[19] E. Reehuis and T. Bäck, "Mixed-integer evolution strategy using multiobjective selection applied to warehouse design optimization, Proceedings of the 12th annual conference on Genetic and evolutionary computation, New York: ACM, 2010, p. 1187.

[20] R. U. Lenke, A contribution to the design of isolated DC-DC converters for utility applications, 1st ed. Aachen, Ph.D. dissertation, E.ON Energy Research Center, 2012.